

# Task-Specific Normalization for Continual Learning of Blind Image Quality Models

Weixia Zhang, *Member, IEEE*, Kede Ma, *Senior Member, IEEE*, Guangtao Zhai, *Senior Member, IEEE*, and Xiaokang Yang, *Fellow, IEEE*

**Abstract**—In this paper, we present a simple yet effective continual learning method for blind image quality assessment (BIQA) with improved quality prediction accuracy, plasticity-stability trade-off, and task-order-/length robustness. The key step in our approach is to freeze all convolution filters of a pre-trained deep neural network (DNN) for an explicit promise of stability, and learn task-specific normalization parameters for plasticity. We assign each new IQA dataset (*i.e.*, task) a prediction head, and load the corresponding normalization parameters to produce a quality score. The final quality estimate is computed by a weighted summation of predictions from all heads with a lightweight  $K$ -means gating mechanism. Extensive experiments on six IQA datasets demonstrate the advantages of the proposed method in comparison to previous training techniques for BIQA.

**Index Terms**—Blind image quality assessment, continual learning, task-specific normalization.

## I. INTRODUCTION

THERE is an emerging trend to develop image quality assessment (IQA) models [1] and image processing methods in alternation: Better IQA models provide more reliable guidance to the design and optimization of the latter, while new image processing algorithms call for the former to handle novel visual artifacts. This suggests a desirable IQA model to easily adapt to such distortions by continually learning from new data (see Fig. 1).

This paper focuses on continual learning of blind IQA (BIQA) models [2], [3], which predict the perceptual quality of a “distorted” image without reference to an original undistorted counterpart. Over the past 20 years, the research in BIQA has shifted from handling distortion-specific [4], single-stage [5], synthetic artifacts to general-purpose [6], multi-stage [7], authentic ones, and from relying on handcrafted features to purely data-driven approaches [8]. Existing BIQA models are generally developed and tested using human-rated images from the same dataset, *i.e.*, within the same subpopulation [2]. As such, even the best-performing BIQA methods, *e.g.*, those based on deep neural networks (DNNs) are bound to encounter subpopulation shift when deployed in the real world.

Direct fine-tuning model parameters with new data may result in *catastrophic forgetting* [9], [10] of previously seen

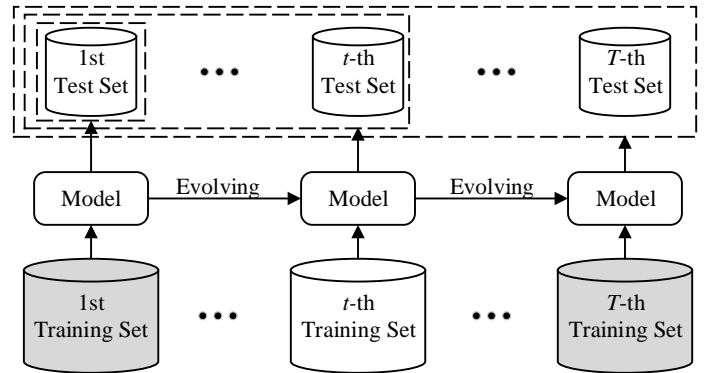


Fig. 1. Illustration of continual learning for BIQA. The grey cylinders denote the inaccessibility of previous and future training data. During testing, we use all previous and the current test sets (indicated by dashed rectangles) to evaluate the stability and plasticity of the learned BIQA model.

data. The dataset combination trick in [11] has been proven effective in handling subpopulation shift, but is limited by the computational scalability and the dataset accessibility. Recently, Zhang *et al.* [2] formulated continual learning for BIQA with five desiderata. They also described the first continual learning method of training BIQA models based on a technique called learning with forgetting (LwF) [12]. Like many continual learning methods (for classification), LwF adds a form of regularization [13] to mildly adjust model parameters for new tasks while respecting old tasks. Nevertheless, this type of regularization-based methods have two limitations. First, it is practically difficult to set the trade-off parameter for stability (*i.e.*, the ability to consolidate acquired knowledge from old tasks) and plasticity (*i.e.*, the ability to learn new knowledge from the current task). Second, the performance is usually sensitive to the order and the length of the task sequence [2], [14].

In this paper, we describe a simple yet effective continual learning method for BIQA based on parameter decomposition. We start with a pre-trained DNN as the feature extractor. We freeze all convolution filters, and share them along with all parameter-free nonlinear activation and pooling layers across tasks during the entire continual learning process. We append a prediction head, implemented by a fully connected (FC) layer, when learning a new task. We allow the parameters of batch normalization (BN) [15] following each convolution to be specifically learned for each task. Through this *task-specific* normalization, a better plasticity-stability trade-off can be made with a negligible increase in model size. During

Weixia Zhang, Guangtao Zhai, and Xiaokang Yang are with the MoE Key Lab of Artificial Intelligence, AI Institute, Shanghai Jiao Tong University, Shanghai, China (e-mail: zwx8981@sjtu.edu.cn; zhaiguangtao@sjtu.edu.cn; xkyang@sjtu.edu.cn).

Kede Ma is with the Department of Computer Science and Shenzhen Research Institute, City University of Hong Kong, Kowloon, Hong Kong (e-mail: kede.ma@cityu.edu.hk).

inference, we load each group of BN parameters to produce a quality estimate using the corresponding prediction head. The final quality score is computed by a weighted summation of predictions from all heads with a lightweight  $K$ -means gating (KG) mechanism.

In summary, our contributions are threefold.

- We propose a new continual learning method for BIQA. The resulting method, which we name TSN-IQA, integrates new knowledge into BN parameters without catastrophic forgetting of acquired knowledge.
- We design a lightweight KG module that only requires learning a set of distortion-aware BN parameters (instead of relying on an extra DNN [2]) to compute the weightings of prediction heads during inference.
- We perform extensive experiments to demonstrate the advantages of our method in terms of quality prediction accuracy, plasticity-stability trade-off, and task-order/length robustness.

## II. RELATED WORK

In this section, we give an overview of recent progress in BIQA. We then review representative continual learning methods for classification, and discuss normalization techniques in the broader context of deep learning.

### A. BIQA Models

Many early BIQA methods are based on hand-engineered natural scene statistics (NSS) in spatial [6], [16], transformed [17], or both domains [18]. In recent years, deep learning began to show its promise in the field of BIQA. Patchwise training [8], [19], transfer learning [20], and quality-aware pre-training [21]–[23] were proposed to compensate for the lack of human-rated data. Of particular interest is the introduction of IQA datasets with realistic distortions [24]–[26], which excites a series of BIQA models to address the synthetic-to-real generalization. Zhang *et al.* [27] assembled two network branches to account for synthetic and realistic distortions separately. Su *et al.* [28] investigated content-aware convolution for robust BIQA, while Zhu *et al.* [29] aimed to learn more transferable quality-aware representations by meta-learning. Zhang *et al.* [11] proposed a dataset combination strategy to train BIQA models on multiple IQA datasets. They later formulated the continual learning setting for BIQA, and introduced a method that combines LwF [12] with a  $K$ -means gating (KG) module [2]. Concurrently, Liu *et al.* [3] proposed a continual learning method for BIQA based on a replay strategy. Ma *et al.* [30] relied on model pruning techniques to enable continual learning of BIQA methods.

In this paper, we follow the setting in [2], and propose a new continual learning method for BIQA with significantly improved performance in several aspects.

### B. Continual Learning for Classification

While humans rarely forget previously learned knowledge catastrophically, machine learning models such as DNNs tend

to do so when learning new concepts [10], [31]. Enforcing regularization is a common practice to mitigate the catastrophic forgetting problem in continual learning. For example, Li and Hoiem [12] proposed LwF, which leverages model predictions of previous tasks as pseudo labels. Elastic weight consolidation (EWC) [32], variational continual learning (VCL) [33], synaptic intelligence (SI) [34], and memory-aware synapses (MAS) [35] work similarly by identifying and penalizing changes to important parameters of previous tasks. From this perspective, parameter decomposition [13] can be seen as a form of hard regularization, disentangling model parameters into task-agnostic and task-specific groups. This may be done by either masking learned parameters of previous tasks [36]–[38] or growing new branches to accommodate new tasks [39]. For example, Yoon *et al.* [14] proposed additive parameter decomposition to achieve task-order robustness. Singh *et al.* [40] calibrated the convolution responses of a continually trained DNN with a few parameters for new tasks. In this paper, we take a similar but much simpler parameter decomposition approach to achieve accurate and robust continual learning for BIQA.

### C. Normalization in Deep Learning

There is increasing evidence that normalization is a canonical neural computation throughout the visual system, and in many other sensory modalities and brain regions [41]. As biologically inspired, deep learning also incorporates different instantiations of normalization for various purposes, such as accelerating model training [15] and improving model generalization [42]. BN is a popular technique to improve the training efficiency of DNNs, in which the convolution responses are divided by the standard deviation (std) of a pool of responses along the batch (and spatial) dimensions. Xie *et al.* [43] learned separate BN layers to harness adversarial examples, which improves image recognition models. Li *et al.* [44] proposed adaptive BN for domain adaptation, assuming that domain-invariant and domain-specific computations are learned by the convolution filters and the BN layers, respectively. Chang *et al.* [45] specialized BN layers using a two-stage algorithm for unsupervised domain adaptation. Dumoulin *et al.* [46] relied on conditional instance normalization [47] to synthesize the artistic styles of diverse paintings. Zhang *et al.* [48] presented a passport normalization for deep model intellectual property protection. In this paper, we introduce task-specific BN to accomplish continual learning of DNN-based BIQA models.

## III. PROPOSED METHOD

In this section, we first revisit the formulation of continual learning for BIQA in [2], and then elaborate the training and inference procedures of the proposed TSN-IQA. To facilitate mathematical comprehension, we summarize a list of variables in Table III-A.

### A. Problem Formulation

When training on the  $t$ -th dataset  $\mathcal{D}_t$ , *i.e.*, the  $t$ -th task, a BIQA model  $f_w$ , parameterized by a vector  $w$ , has no direct

TABLE I  
LIST OF VARIABLES

Notation	Description
$(x, y)$	an image pair
$(\mu_x, \mu_y)$	MOSs of $x$ and $y$
$\mathcal{D}_t$	the $t$ -th dataset
$\mathcal{P}_t$	the $t$ -th paired dataset
$N_t$	# of image pairs in the $t$ -th paired dataset
$f_\phi$	a DNN parameterized by a vector $\phi$
$h_{\psi_t}$	the $t$ -th prediction head parameterized by $\psi_t$
$r(x, y)$	the binary quality label of $(x, y)$
$\hat{p}_t(x, y)$	the predicted probability of $(x, y)$ for the $t$ -th task
$(\mu_t, \sigma_t, \gamma_t, \beta_t)$	the 4-tuple BN parameters for the $t$ -th task
$c_{kst}$	the $k$ -th centroid at the $s$ -th stage for the $t$ -th task
$d_{st}(x)$	the perceptual relevance of $x$ to the $t$ -th task
$a_{st}(x)$	the weighting of $x$ for the $t$ -th prediction head
$\hat{q}(x)$	the predicted quality score of $x$

access to previous training images in  $\{\mathcal{D}_k\}_{k=1}^{t-1}$ , leading to the following objective:

$$\mathcal{L}(\mathcal{D}_t; w) = \frac{1}{|\mathcal{D}_t|} \sum_{(x, \mu_x) \in \mathcal{D}_t} \ell(f_w(x), \mu_x) + \lambda \Omega(w), \quad (1)$$

where  $x$  and  $\mu_x$  denote the ‘‘distorted’’ image and the corresponding mean opinion score (MOS), respectively.  $\ell(\cdot)$  is a quantitative measure of quality prediction performance, and  $\Omega(\cdot)$  is an optional regularizer. A good BIQA model under this setting should adapt well to new tasks, and meanwhile endeavor to mitigate catastrophic forgetting of old tasks as measured by

$$\sum_{k=1}^t \mathcal{L}(\mathcal{V}_k; w) = \sum_{k=1}^t \left( \frac{1}{|\mathcal{V}_k|} \sum_{(x, \mu_x) \in \mathcal{V}_k} \ell(f_w(x), \mu_x) \right), \quad (2)$$

where  $\mathcal{V}_k$  denotes the test set for the  $k$ -th task. Five desiderata are suggested in [2] to make continual learning for BIQA feasible and nontrivial: 1) common perceptual scale, 2) robust to subpopulation shift, 3) limited access to previous data, 4) no test-time oracle, and 5) bounded memory footprint.

### B. Model Estimation

Inspired by UNIQUE [11], we exploit relative quality information to learn a common perceptual scale for all tasks. Specifically, given an image pair  $(x, y)$ , we compute a binary label:

$$r(x, y) = \begin{cases} 1 & \text{if } \mu_x \geq \mu_y \\ 0 & \text{otherwise} \end{cases}. \quad (3)$$

Careful readers may find that we do not infer a continuous value  $p(x, y)$ , which denotes the probability of  $x$  perceived better than  $y$  based on the Thurstone’s model [49] or the Bradley-Terry model [50] as typically done in previous work [11], [23]. This is because the computed probability may vary with the precision of the subjective testing methodology. For example, if  $x$  is marginally better than  $y$  and a precise subjective method such as the two-alternative forced choice (2AFC) is adopted,  $p(x, y)$  can be close to one. By contrast, if a less precise subjective method such as the single stimulus continuous quality rating is used,  $p(x, y)$  may only be slightly

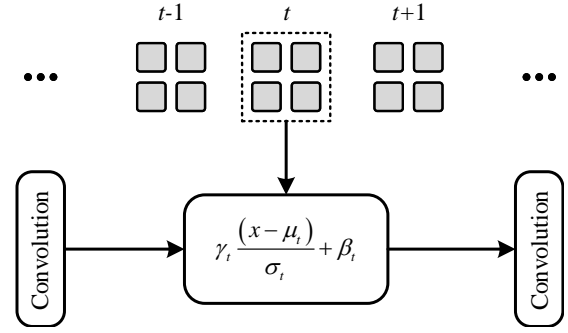


Fig. 2. Illustration of task-specific BN. The parameters of all convolutions are frozen and shared across all tasks. A group of BN parameters is customized for each task.

larger than 0.5. Compared to  $p(x, y)$ , we also empirically observe that  $r(x, y)$  leads to faster convergence and improved accuracy results. When learning the  $t$ -th task, we transform  $\mathcal{D}_t = \{x_i^{(i)}, \mu_t^{(i)}\}_{i=1}^{|\mathcal{D}_t|}$  to  $\mathcal{P}_t = \{(x_t^{(i)}, y_t^{(i)}), r_t^{(i)}\}_{i=1}^{N_t}$ , where  $N_t \leq \binom{|\mathcal{D}_t|}{2}$ .

Our BIQA model consists of a feature extractor implemented by a DNN,  $f_\phi(\cdot)$ , producing a fixed-length image representation independent of input resolution. For the  $t$ -th task, we append a prediction head implemented by an FC layer,  $h_{\psi_t}(\cdot)$ , outputting a corresponding quality score. Under the Thurstone’s Case V model [49], we estimate the probability that  $x$  is of higher quality than  $y$  by

$$\hat{p}_t(x, y) = \Phi \left( \frac{h_{\psi_t}(f_\phi(x)) - h_{\psi_t}(f_\phi(y))}{\sqrt{2}} \right), \quad (4)$$

where the quality prediction variance is fixed to one. We measure the statistical distance between the ground-truth labels and predicted probabilities using the fidelity loss [51] due to its favorable optimization behaviors [11]:

$$\ell(x, y; \phi, \psi_t) = 1 - \sqrt{r(x, y)\hat{p}_t(x, y)} - \sqrt{(1 - r(x, y))(1 - \hat{p}_t(x, y))}. \quad (5)$$

To make a better trade-off between plasticity and stability while keeping a bounded model size, our BIQA method chooses to maximally share computation across tasks, and customize a tiny fraction of parameters to account for the incremental difference introduced by new tasks. In particular, our feature extractor is composed of several stages of convolution, BN, halfwave-rectification (*i.e.*, ReLU nonlinearity), and max-pooling. We freeze all pre-trained convolution parameters during model development, and learn a group of 4-tuple BN parameters for the  $t$ -th task

$$z_{\text{BN}} = \gamma_t \left( \frac{z - \mu_t}{\sigma_t} \right) + \beta_t, \quad (6)$$

where  $\mu_t$  and  $\sigma_t$  are the mean and the std estimated by the exponentially decaying moving average over mini-batches.  $\gamma_t$  and  $\beta_t$  are the learnable scaling and shift parameters (see also Fig. 2). After training on a  $T$ -length task sequence, we obtain  $T$  groups of task-specific BN parameters.

### C. Model Inference

During inference, we successively load each of  $T$  groups of BN parameters along with the corresponding FC layer to compute  $T$  quality scores. Due to the unavailability of the task oracle, we rely on an improved KG module [2] with a lightweight design goal, which is made possible by the proposed parameter decomposition scheme. Unlike [2], we only train a set of task-agnostic BN parameters on a large-scale image set with various synthetic distortions [27] for distortion-aware weighting computation, while keeping all convolution filters intact. Since the original BN parameters of the pre-trained feature extractor are not necessary, our gating mechanism introduces essentially no extra parameters, and adheres to the desideratum of bounded memory footprint.

We present the overview of the inference process in Fig. 3. During learning the  $t$ -th task, we load the distortion-aware BN parameters to the pre-trained  $f_\phi$  to compute globally pooled convolution responses of image  $x$  at the  $s$ -th stage,  $\bar{f}_{\phi_s}(x)$ . Given  $S$ -stage convolutions, we obtain a feature summary of  $\mathcal{D}_t$ :  $\{\bar{f}_{\phi_1}(x_t^{(i)}), \dots, \bar{f}_{\phi_S}(x_t^{(i)})\}_{i=1}^{|\mathcal{D}_t|}$ . We then apply  $K$ -means [52] (for each stage of convolution responses) to compute  $S$  groups of  $K$  centroids  $\{c_{kst}\}_{k=1}^K\}_{s=1}^S$ .

We measure the perceptual relevance of  $x$  to  $\mathcal{D}_t$  by computing the minimal Euclidean distances between  $\bar{f}_{\phi_s}(x)$  and  $\{c_{kst}\}_{k=1}^K$ :

$$d_{st}(x) = \min_k \|\bar{f}_{\phi_s}(x) - c_{kst}\|_2. \quad (7)$$

We pass  $\{d_{st}(x)\}_{t=1}^T$  to a softmax function to compute the weightings at the  $s$ -th stage for the  $t$ -th prediction head:

$$a_{st}(x) = \frac{\exp(-\tau d_{st}(x))}{\sum_{t=1}^T \exp(-\tau d_{st}(x))}, \quad (8)$$

where  $\tau \geq 0$  is a parameter to control the smoothness of the softmax function. We further average the weightings across stages to obtain

$$a_t(x) = \frac{1}{S} \sum_s a_{st}(x). \quad (9)$$

We last compute the overall quality score by the inner product between the weighting and quality prediction vectors:

$$\hat{q}(x) = \sum_{t=1}^T a_t(x) h_{\psi_t}(f_\phi(x)). \quad (10)$$

## IV. EXPERIMENTS

In this section, we first describe the experimental setups for continual learning of BIQA models, and then compare the proposed TSN-IQA against previous training techniques, supplemented by abundant ablation studies. The source code is made publicly available at <https://github.com/zwx8981/TSN-IQA> for reproducible research.

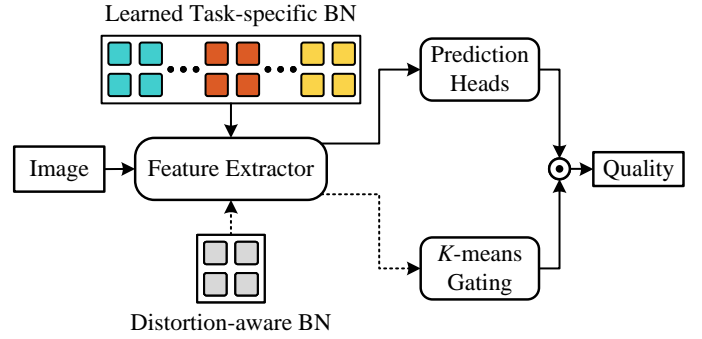


Fig. 3. Overview of the inference process. The solid line indicates the pipeline of loading task-specific BN parameters learned for different tasks (denoted by different colors) and making the quality prediction using the corresponding prediction heads. The dotted line indicates the process of loading distortion-aware BN parameters and computing weightings for all prediction heads with the KG module.

### A. Experimental Setups

We select six widely used IQA datasets: LIVE [5], CSIQ [56], BID [24], LIVE Challenge [25], KoniQ-10K [26], and KADID-10K [57]. We summarize the details of the six datasets in Table II. In general, the number of training pairs is proportional to the number of images in the training set of each dataset.

Following [2], we organize these datasets in chronological order for the main experiments. We randomly sample 70% and 10% images from each dataset for training and validation, respectively, and leave the remaining for testing. To ensure content independence in LIVE, CSIQ, and KADID-10K, we divide the training and test sets according to the reference images.

We choose a variant of ResNet-18 [58] as the feature extractor. We keep the front convolution and four residual blocks, which are indexed by Stage 1 to Stage 4, respectively. We append an FC layer as the prediction head on top of the convolution response from Stage 4, and compute the weightings using the convolution responses from later two stages. As such, 10,112 learnable parameters are introduced by BN and FC layers for each new task, accounting for less than 0.18% of the total network parameters. During inference, the number of centroids used in  $K$ -means is set to  $K = 128$  for each new task<sup>1</sup>, which introduces 98,304 parameters for additional memory budget, accounting for about 0.88% of the backbone network parameters. Putting together, the current configuration ensures that TSN-IQA conforms to the bounded memory footprint desideratum.

For each task, stochastic optimization is carried out by Adam [59] with an initial learning rate of  $1 \times 10^{-3}$ . We decay the learning rate by a factor of 10 at the 8-th epoch, and train our method for a maximum of twelve epochs. We set the temperature to  $\tau = 32$  in Eq. (8). We test on images of the original size.

We use Spearman's rank correlation coefficient (SRCC) to measure the prediction performance. When continually learning a BIQA model on a  $T$ -length task sequence, we

<sup>1</sup>Empirically, we find that TSN-IQA is insensitive to the choice of  $K$ .

TABLE II

SUMMARY OF IQA DATASETS USED IN OUR EXPERIMENTS. CLIVE STANDS FOR THE LIVE CHALLENGE DATABASE. TID2013 [53], SPAQ [54], AND AGIQA-3K [55] ARE USED FOR CROSS-DATABASE EVALUATION. SS: SINGLE STIMULUS. DS: DOUBLE STIMULUS. MS: MULTIPLE STIMULUS. CQR: CONTINUOUS QUALITY RATING. ACR: ABSOLUTE CATEGORY RATING. CS: CROWDSOURCING. PC: PAIRED COMPARISON

Dataset	# of Images	# of Training Pairs	# of Test Images	Scenario	# of Types	Testing Methodology	Year
LIVE [5]	779	7,780	163	Synthetic	5	SS-CQR	2006
CSIQ [56]	866	8,786	173	Synthetic	6	MS-CQR	2010
BID [24]	586	11,204	117	Realistic	N.A.	SS-CQR	2011
CLIVE [25]	1,162	24,604	232	Realistic	N.A.	SS-CQR-CS	2016
KonIQ-10K [26]	10,073	139,274	2,015	Realistic	N.A.	SS-ACR-CS	2018
KADID-10K [57]	10,125	140,071	2,000	Synthetic	25	DS-ACR-CS	2019
TID2013 [53]	3,000	N.A.	3,000	Synthetic	25	DS-PC	2013
SPAQ [54]	11,125	N.A.	11,125	Realistic	N.A.	SS-CQR	2020
AGIQA-3K [55]	2,982	N.A.	2,982	Generated	N.A.	SS-CQR	2023

TABLE III

PERFORMANCE COMPARISON IN TERMS OF mSRCC, mPI, mSI, AND mPSI. TASK-AWARE AND TASK-AGNOSTIC EVALUATION SETTINGS CORRESPOND TO QUALITY PREDICTION WITH AND WITHOUT THE TASK ORACLE, RESPECTIVELY. ALL METHODS ARE TRAINED IN CHRONOLOGICAL ORDER

Setting	Backbone	ResNet-18				Two-Stream DNN			
	Method	mSRCC	mPI	mSI	mPSI	mSRCC	mPI	mSI	mPSI
Task-Aware	SI-O	0.786	<b>0.858</b>	0.886	0.872	0.834	<b>0.881</b>	0.947	0.914
	MAS-O	0.779	0.853	0.882	0.868	0.835	0.874	0.955	0.915
	LwF-O	0.804	0.841	0.970	0.906	0.849	0.877	0.986	<b>0.931</b>
	TSN-IQA-O	<b>0.855</b>	0.855	<b>1.000</b>	<b>0.928</b>	<b>0.862</b>	0.862	<b>1.000</b>	<b>0.931</b>
Task-Agnostic	SL	0.666	0.851	0.751	0.801	0.677	0.876	0.805	0.840
	SI	0.762	<b>0.858</b>	0.876	0.867	0.732	<b>0.881</b>	0.822	0.852
	SI-KG	0.778	0.856	0.877	0.867	0.785	0.877	0.932	0.900
	MAS	0.717	0.853	0.862	0.858	0.617	0.874	0.797	0.836
	MAS-KG	0.769	0.854	0.872	0.863	0.780	0.862	0.943	0.903
	LwF	0.691	0.841	0.890	0.866	0.669	0.877	0.833	0.855
	LwF-KG	0.801	0.837	0.963	0.900	0.815	0.856	0.980	0.918
	TSN-IQA	<b>0.846</b>	0.853	<b>0.979</b>	<b>0.916</b>	<b>0.846</b>	0.860	<b>0.985</b>	<b>0.923</b>

compute the mean SRCC between model predictions and MOSs of each dataset as a measure of prediction accuracy:

$$\text{mSRCC} = \frac{1}{T} \sum_{k=1}^T \text{SRCC}_{Tk}, \quad (11)$$

where  $\text{SRCC}_{tk}$  is the SRCC result of the  $t$ -th model on the  $k$ -th dataset. We then compute a mean plasticity index (mPI):

$$\text{mPI} = \frac{1}{T} \sum_{t=1}^T \text{PI}_t = \frac{1}{T} \sum_{t=1}^T \text{SRCC}_{tt}, \quad (12)$$

*i.e.*, the average result of the model on the current dataset along the task sequence, and a mean stability index (mSI) by measuring the variability of model performance on old data when learning on a new task:

$$\text{mSI} = \frac{1}{T} \sum_{t=1}^T \text{SI}_t, \quad (13)$$

where

$$\text{SI}_t = \begin{cases} 1 & t = 1 \\ \frac{1}{t-1} \sum_{k=1}^{t-1} \widehat{\text{SRCC}}_{tk} & t > 1 \end{cases}, \quad (14)$$

where  $\widehat{\text{SRCC}}_{tk}$  for  $k < t$  is computed between the predictions of the  $t$ -th and  $k$ -th models. mSRCC, mPI, and mSI measure different and complementary aspects of a continually learned BIQA model. We also quantify the plasticity-stability trade-off

using a mean plasticity-stability index (mPSI) over a list of  $T$  tasks:

$$\text{mPSI} = \frac{1}{T} \sum_{t=1}^T \text{PSI}_t = \frac{1}{2T} \sum_{t=1}^T (\text{PI}_t + \text{SI}_t). \quad (15)$$

## B. Competing Methods

We describe several competing methods for training. For a fair comparison, we rely on the same backbone network (*i.e.*, ResNet-18) as TSN-IQA for implementation. We further instantiate TSN-IQA using a two-stream DNN, composed of a variant of ResNet-18 and a VGG-like network, which allows for a direct performance comparison with other methods that share the setup in [2].

- **Separate Learning (SL)** is the standard in BIQA, which trains the model using a single prediction head on one of the six training sets.
- **Joint Learning (JL)** refers to the dataset combination trick [11] to address the cross-distortion-scenario challenge in BIQA. As an upper bound of all continual learning methods, JL trains the model with a single head on the combination of all six training sets.
- **LwF** [12] in BIQA is based on a multi-head architecture, which introduces a stability regularizer that uses the previous model outputs as soft labels to preserve the performance of previously seen data. LwF relies on the

TABLE IV

PERFORMANCE COMPARISON IN TERMS OF SRCC. BEST RESULTS IN EACH SECTION ARE HIGHLIGHTED IN BOLD, AND RESULTS OF FUTURE TASKS ARE MARKED IN GREY. ALL METHODS EMPLOY A VARIANT OF RESNET-18 AS THE BACKBONE NETWORK

Dataset	Method	LIVE [5]	CSIQ [56]	BID [24]	CLIVE [25]	KonIQ-10K [26]	KADID-10K [57]
All	JL	0.969	0.815	0.842	0.827	0.856	0.896
LIVE	SL	0.927	0.645	0.726	0.407	0.645	0.556
	LwF	0.927	0.645	0.726	0.407	0.645	0.556
	LwF-KG	0.927	0.645	0.726	0.407	0.645	0.556
	SI	0.927	0.645	0.726	0.407	0.645	0.556
	SI-KG	0.927	0.645	0.726	0.407	0.645	0.556
	MAS	0.927	0.645	0.726	0.407	0.645	0.556
	MAS-KG	0.927	0.645	0.726	0.407	0.645	0.556
	TSN-IQA	<b>0.956</b>	0.677	0.645	0.465	0.680	0.504
CSIQ	SL	0.903	0.846	0.656	0.426	0.628	0.552
	LwF	<b>0.954</b>	0.805	0.692	0.440	0.684	0.581
	LwF-KG	0.923	0.815	0.725	0.472	0.680	0.530
	SI	0.953	<b>0.880</b>	0.596	0.415	0.646	0.575
	SI-KG	0.940	0.874	0.596	0.414	0.643	0.554
	MAS	0.948	0.874	0.617	0.412	0.659	0.581
	MAS-KG	0.935	0.870	0.617	0.412	0.658	0.566
	TSN-IQA	0.950	0.850	0.672	0.477	0.696	0.522
BID	SL	0.716	0.569	0.766	0.660	0.645	0.374
	LwF	0.938	0.792	0.782	0.572	0.729	0.547
	LwF-KG	0.920	0.796	0.789	0.511	0.718	0.528
	SI	0.886	0.835	<b>0.814</b>	0.562	0.718	0.571
	SI-KG	0.885	0.839	0.813	0.536	0.717	0.570
	MAS	0.907	0.826	0.785	0.556	0.682	0.595
	MAS-KG	0.841	0.833	0.785	0.541	0.685	0.594
	TSN-IQA	<b>0.952</b>	<b>0.855</b>	0.812	0.720	0.701	0.494
CLIVE	SL	0.448	0.472	<b>0.839</b>	<b>0.836</b>	0.756	0.306
	LwF	0.814	0.646	0.820	0.802	0.774	0.522
	LwF-KG	0.910	0.776	0.785	0.776	0.756	0.552
	SI	0.925	0.792	0.804	0.809	0.804	0.536
	SI-KG	0.929	0.800	0.807	0.811	0.803	0.527
	MAS	0.911	0.759	0.818	0.821	0.776	0.497
	MAS-KG	0.928	0.770	0.828	0.821	0.774	0.496
	TSN-IQA	<b>0.953</b>	<b>0.837</b>	0.833	0.799	0.730	0.502
KonIQ-10K	SL	0.785	0.708	0.768	0.723	<b>0.895</b>	0.593
	LwF	0.868	0.705	0.768	0.725	0.889	0.598
	LwF-KG	0.913	0.741	0.800	0.779	0.870	0.617
	SI	0.850	0.708	0.781	0.713	0.888	0.608
	SI-KG	0.884	0.693	0.793	0.739	0.885	0.611
	MAS	0.901	0.712	0.775	0.693	0.883	0.613
	MAS-KG	0.936	0.716	0.797	0.737	0.880	0.620
	TSN-IQA	<b>0.959</b>	<b>0.813</b>	<b>0.823</b>	<b>0.796</b>	0.869	0.568
KADID-10K	SL	0.881	0.639	0.635	0.387	0.618	0.835
	LwF	0.853	0.736	0.676	0.418	0.622	0.842
	LwF-KG	0.888	0.731	0.766	0.741	0.831	<b>0.849</b>
	SI	0.895	0.761	0.740	0.612	0.731	0.832
	SI-KG	0.871	0.742	0.782	0.687	0.764	0.824
	MAS	0.876	0.744	0.753	0.419	0.677	0.831
	MAS-KG	0.857	0.758	0.808	0.600	0.752	0.840
	TSN-IQA	<b>0.954</b>	<b>0.801</b>	<b>0.829</b>	<b>0.786</b>	<b>0.870</b>	0.830

newest head for quality prediction. We also leverage the task oracle to select the corresponding head for quality prediction, denoted by **LwF-O**.

- **LwF-KG** [2] uses a modified LwF [12] for training and the KG mechanism for inference.
- **SI** [34] is also a regularization-based continual learning method, which estimates important parameters for previous tasks.

Similar to LwF, we implement a multi-head architecture for SI, and rely on the newest head to predict image quality. We try to improve the performance with the KG mechanism, denoted by **SI-KG**, and leverage the task oracle as well, denoted by **SI-O**.

- **MAS** [34] shares a similar philosophy with SI to penalize

the changes to important weights. The difference lies only in the calculation of the cumulative importance measure. Similarly, MAS uses the latest head for quality prediction, and has two variants that include the KG module and the task oracle, denoted by **MAS-KG** and **MAS-O**, respectively.

- **TSN-IQA** makes use of task-specific BN to handle new tasks, and enhances the KG module in [2] using rich feature hierarchies with less memory footprint. We also replace the KG module with the task oracle for quality prediction, denoted by **TSN-IQA-O**.

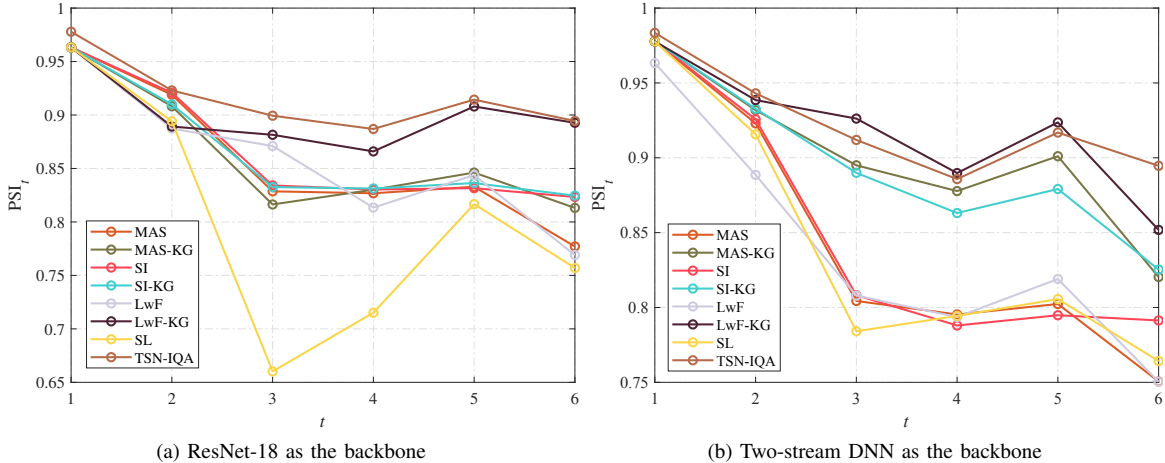


Fig. 4.  $PSI_t$  as a function of the task index  $t$ .

### C. Main Results

Table III lists mSRCC, mPI, mSI, and mPSI results on the six IQA test sets. Several interesting observations have been made. First, without any remedy for catastrophic forgetting, the performance of SL is far from satisfactory, consistent with previous findings [2]. Particularly, we identify a significant performance drop when SL transits from CSIQ to BID (see Table IV), where an apparent subpopulation shift from synthetic to realistic distortions is introduced. Second, direct application of LwF, SI, and MAS from image classification to BIQA achieves significantly better performance over SL in terms of mSI and similar performance in terms of mPI.

Third, equipped with the KG module, LwF-KG, SI-KG, and MAS-KG outperform their counterparts in terms of both mSRCC and mPSI. The performance is even comparable to their “upper bounds” (*i.e.*, LwF-O, SI-O, and MAS-O) under all evaluation measures. Notably, compared to TSN-IQA which shares the majority of parameters between the feature extractor and the KG module, these models require twice more memory budget. Fourth, TSN-IQA-O achieves the best results, which outperforms LwF-O, SI-O, and MAS-O in terms of mSRCC and mPSI by large margins, and serves as the “upper bound” of TSN-IQA for further improvement. Fifth, both LwF-KG and TSN-IQA demonstrate improved performance regarding the plasticity/stability trade-off by switching ResNet-18 to a more advanced two-stream DNN. Sixth, when the task oracle is available, LwF-O is comparable to TSN-IQA-O for the two-stream backbone. But, this is not the case when ResNet-18 is the backbone, where TSN-IQA-O significantly surpasses LwF-O. This indicates that TSN-IQA is more resilient to changes in the backbone architecture. Lastly, TSN-IQA consistently outperforms LwF-KG [2] in terms of mPSI and mSRCC when using the same backbone network (ResNet-18 or the two-stream DNN), verifying the technical contribution of the proposed approach.

We plot  $PSI_t$  as a function of the task index  $t$  in Fig. 4, from which we find our method is more stable as the length of the task sequence grows for different backbone networks. We then look closely at the performance variations along the

task sequence, and summarize the SRCC results continually in Table IV.

Several useful findings are worth mentioning. First, JL provides an effective but unscalable solution to the subpopulation shift in BIQA, serving as the upper bound of all continual learning methods. Second, the plasticity of SL is reasonably good, but the results on previously learned tasks suffer from significant oscillations due to the subpopulation shift between synthetic and realistic distortions [11], [20], [27]. Third, the favorable performance of LwF-KG, SI-KG, and MAS-KG against LwF, SI, and MAS especially on old tasks validates the KG module for summarizing quality predictions.

We last conduct a qualitative analysis of our BIQA model by showing representative test images from the task sequence in Fig. 5. We find that for frequently-seen distortion appearances (*e.g.*, global blurring in (a)), all heads tend to make reasonable predictions, and more weightings are given to the corresponding head. Meanwhile, if one distortion type occurs in multiple datasets (*e.g.*, JPEG2000 compression in (b)), the heads that have seen the distortion work well, while others do not. Fortunately, the KG module is able to underweight inaccurate heads. Moreover, TSN-IQA successfully aligns images of synthetic and realistic distortions in a common perceptual scale, despite not being exposed to pairs of images from different distortion scenarios.

### D. Results of Task-Order-/Length Robustness

In real-world applications, novel distortions may emerge in arbitrary order. As a result, a continual learning method for BIQA is expected to be robust to different task orders. In addition to (I) the default chronological order, we experiment with seven more task orders: (II) synthetic and realistic distortions in alternation: LIVE  $\rightarrow$  BID  $\rightarrow$  CSIQ  $\rightarrow$  LIVE Challenge  $\rightarrow$  KADID-10K  $\rightarrow$  KonIQ-10K, (III) synthetic distortions followed by realistic distortions: LIVE  $\rightarrow$  CSIQ  $\rightarrow$  KADID-10K  $\rightarrow$  BID  $\rightarrow$  LIVE Challenge  $\rightarrow$  KonIQ-10K, (IV) realistic distortions followed by synthetic distortions: BID  $\rightarrow$  LIVE Challenge  $\rightarrow$  KonIQ-10K  $\rightarrow$  LIVE  $\rightarrow$  CSIQ  $\rightarrow$  KADID-10K, and (V)-(VIII) the reverses of Orders (I)-(IV).

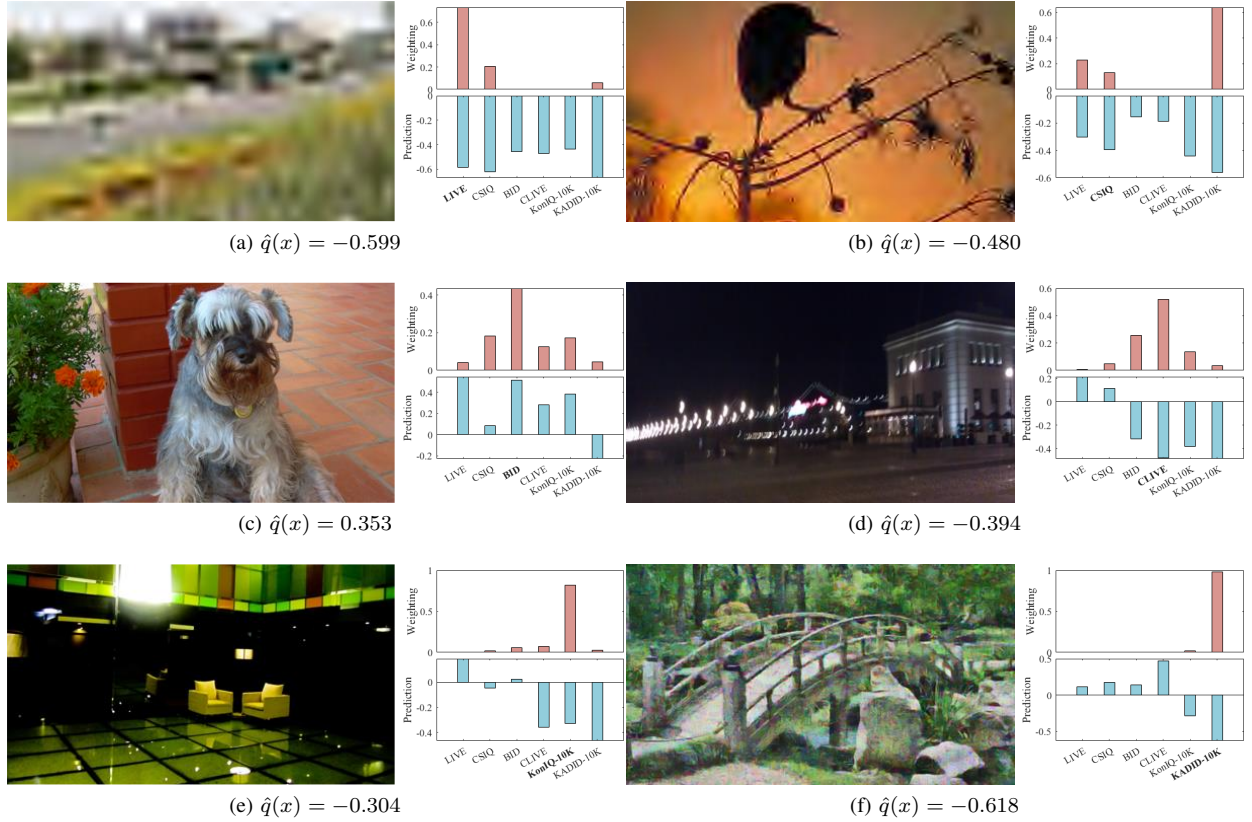


Fig. 5. Learned common perceptual scale to embed images from the six IQA datasets. The bar charts of weightings and quality predictions are also presented alongside each image. The dataset in bold indicates the origin of the test image. The final quality prediction  $\hat{q}(x)$  is shown in the subcaption. Zoom in for better distortion visibility.

TABLE V

COMPARISON OF TASK-ORDER ROBUSTNESS MEASURED BY mSRCC, mPI, mSI, AND mPSI. I: DEFAULT CHRONOLOGICAL ORDER. II: SYNTHETIC AND REALISTIC DISTORTIONS IN ALTERNATION. III: SYNTHETIC DISTORTIONS FOLLOWED BY REALISTIC DISTORTIONS. IV: REALISTIC DISTORTIONS FOLLOWED BY SYNTHETIC DISTORTIONS. V TO VIII: REVERSES OF ORDERS I TO IV, RESPECTIVELY

Order	I		II		III		IV	
Metric	LwF-KG	TSN-IQA	LwF-KG	TSN-IQA	LwF-KG	TSN-IQA	LwF-KG	TSN-IQA
mSRCC	0.801	<b>0.846</b>	0.807	<b>0.846</b>	0.832	<b>0.846</b>	0.781	<b>0.846</b>
mPI	0.837	<b>0.853</b>	0.836	<b>0.855</b>	0.836	<b>0.852</b>	0.819	<b>0.850</b>
mSI	0.963	<b>0.979</b>	0.957	<b>0.986</b>	0.958	<b>0.979</b>	0.955	<b>0.980</b>
mPSI	0.900	<b>0.916</b>	0.897	<b>0.921</b>	0.897	<b>0.916</b>	0.887	<b>0.915</b>
Order	V		VI		VII		VIII	
Metric	LwF-KG	TSN-IQA	LwF-KG	TSN-IQA	LwF-KG	TSN-IQA	LwF-KG	TSN-IQA
mSRCC	0.803	<b>0.846</b>	0.803	<b>0.846</b>	0.771	<b>0.846</b>	0.808	<b>0.846</b>
mPI	0.841	<b>0.847</b>	0.834	<b>0.850</b>	0.843	<b>0.849</b>	0.829	<b>0.845</b>
mSI	0.959	<b>0.979</b>	0.958	<b>0.989</b>	0.937	<b>0.990</b>	0.962	<b>0.976</b>
mPSI	0.900	<b>0.913</b>	0.896	<b>0.920</b>	0.890	<b>0.920</b>	0.896	<b>0.911</b>

We compare TSN-IQA to LwF-KG [2] in Table V. The main observation is that our method is more robust than LwF-KG for all task orders under all metrics. Furthermore, we note that the results of Orders V and VIII are slightly lower than those of other orders. We believe these arise because we begin with KADID-10K [57], a synthetic dataset that is considered visually much harder than LIVE [5] and CSIQ [56], therefore posing a challenge for performance stabilization. Given a specific task order, we also measure the task-length robustness by the mean mPSI of different lengths,  $\{\text{mPSI}_t\}_{t=1}^T$ . We compare our method to LwF-KG [2] in Table VI. We find the

task-length robustness to be dependent on the task order, and TSN-IQA performs better than LwF-KG across all task orders. A relatively inferior result is observed for Order V, where KADID-10K [57] is listed in the first place. Altogether, these promising results indicate that TSN-IQA has great potential for use in practical quality prediction scenarios.

### E. Ablation Studies

In this subsection, we conduct ablation experiments to probe the performance variations of TSN-IQA. Note that all experiments are conducted using the default chronological order.



TABLE VI  
COMPARISON OF TASK-LENGTH ROBUSTNESS MEASURED BY mPSI FOR DIFFERENT TASK ORDERS

Order Length	I		II		III		IV	
	LwF-KG	TSN-IQA	LwF-KG	TSN-IQA	LwF-KG	TSN-IQA	LwF-KG	TSN-IQA
1	0.963	0.978	0.963	0.978	0.963	0.978	0.882	0.906
2	0.926	0.950	0.929	0.944	0.926	0.950	0.886	0.900
3	0.911	0.933	0.911	0.937	0.915	0.934	0.895	0.907
4	0.900	0.922	0.900	0.926	0.903	0.925	0.901	0.923
5	0.902	0.920	0.898	0.921	0.895	0.916	0.889	0.917
6	0.900	0.916	0.897	0.921	0.898	0.916	0.887	0.915
Mean	0.917	<b>0.937</b>	0.916	<b>0.938</b>	0.897	<b>0.936</b>	0.890	<b>0.911</b>
Order Length	V		VI		VII		VIII	
	LwF-KG	TSN-IQA	LwF-KG	TSN-IQA	LwF-KG	TSN-IQA	LwF-KG	TSN-IQA
1	0.918	0.912	0.946	0.941	0.946	0.941	0.918	0.912
2	0.920	0.918	0.918	0.924	0.923	0.919	0.884	0.906
3	0.903	0.906	0.904	0.913	0.912	0.914	0.896	0.923
4	0.903	0.904	0.886	0.911	0.903	0.912	0.902	0.923
5	0.893	0.902	0.887	0.909	0.887	0.910	0.894	0.913
6	0.900	0.913	0.896	0.919	0.890	0.920	0.896	0.911
Mean	0.906	<b>0.909</b>	0.906	<b>0.920</b>	0.910	<b>0.919</b>	0.898	<b>0.915</b>

TABLE VII  
PERFORMANCE COMPARISON OF TSN-IQA WITH DIFFERENT DESIGN CHOICES. THE RESULTS OF LwF-KG WITH DIFFERENT BACKBONE NETWORKS ARE LISTED AS REFERENCE. THE DEFAULT SETTING IS HIGHLIGHTED IN BOLD

Design Choice		mPSI	mSRCC
LwF-KG (ResNet-18)		0.900	0.801
LwF-KG (Two-Stream DNN)		0.918	0.815
Task-agnostic BN		0.822	0.624
ImageNet Pre-trained BN		0.893	0.835
Feature Hierarchy	Stage 4	0.914	0.839
	Stages <b>3+4</b>	<b>0.916</b>	<b>0.846</b>
	Stages 2+3+4	0.914	0.845
	Stages 1+2+3+4	0.913	0.844
Backbone	VGG-16	0.920	0.845
	ResNet-50	<b>0.924</b>	0.845
	Two-Stream DNN	0.923	<b>0.846</b>

TABLE VIII  
IQA DATASET ANALYSIS VIA PAIRWISE KULLBACK-LEIBLER (KL) DIVERGENCE OF TASK-SPECIFIC BN PARAMETERS. A LOWER VALUE INDICATES THE TWO DATASETS ARE MORE SIMILAR

Dataset	LIVE	CSIQ	BID	CLIVE	KonIQ	KADID
LIVE	0.000	84.680	131.015	144.343	188.037	135.388
CSIQ	81.546	0.000	142.367	152.962	218.956	144.279
BID	101.814	111.335	0.000	63.436	132.474	153.364
CLIVE	123.188	124.207	64.462	0.000	162.499	170.714
KonIQ	110.939	126.010	111.538	122.768	0.000	138.842
KADID	93.250	102.867	134.079	141.610	151.447	0.000

TABLE IX  
SRCC RESULTS OF INTRA- AND INTER-DATASET EVALUATIONS. "INTER-" MEANS THE SET OF BN PARAMETERS (TOGETHER WITH THE CORRESPONDING PREDICTION HEAD) TRAINED FOR ONE TASK ARE TESTED ON OTHER TASKS

Dataset	LIVE	CSIQ	BID	CLIVE	KonIQ	KADID
LIVE	0.956	0.648	0.680	0.453	0.665	0.529
CSIQ	0.893	0.852	0.560	0.383	0.512	0.530
BID	0.682	0.751	0.812	0.691	0.698	0.496
CLIVE	0.534	0.489	0.803	0.807	0.747	0.441
KonIQ	0.687	0.563	0.721	0.646	0.881	0.601
KADID	0.916	0.693	0.618	0.436	0.593	0.824

First, to verify the necessity of the core design of our method - task-specific BN, we train a single group of task-agnostic BN parameters along the task sequence. During inference, we use the converged BN parameters to make predictions for all tasks. As shown in Table VII, this variant achieves an mPSI of 0.822 and an mSRCC of 0.624, which are far below the results by TSN-IQA. We next compare the performance using the ImageNet pre-trained BN with the proposed distortion-aware BN for the KG module. Being exposed to various types of distortions, the distortion-aware BN parameters help the KG module assign weightings to predictions heads more reasonably, leading to higher mPSI and mSRCC results. We then evaluate the influence of the feature hierarchy on the KG module by incorporating different stages of convolution responses. The results in Table VII show that multi-stage features are more beneficial, and the combination of Stage-3 and Stage-4 features delivers the most perceptual gains.

Lastly, we experiment with three different DNNs as the backbone networks, *i.e.*, VGG-16 [61], ResNet-50 [58], and the two-stream DNN [2]. From Table VII, we observe that the proposed parameter decomposition scheme is generic for continual learning of BIQA models, which can be enhanced by working with more powerful backbone networks.

## F. Further Analysis

1) *IQA Dataset Analysis:* During continual learning on a task sequence, TSN-IQA is trained to capture the informative and discriminative information of each task using a group of task-specific BN parameters. It remains to be seen 1) whether the learned BN parameters reflect distinctive aspects of different datasets, and 2) whether they can explain the performance variations. To answer these questions, we first retrieve the exponentially decaying moving averages of the mean and std parameters from the last BN layer learned for each task, which are assumed to follow a multivariate Gaussian distribution. With such  $T$  Gaussian distributions at hand, we compute the pairwise Kullback-Leibler (KL) divergence  $\{\text{KL}_{ij}\}_{i,j=1}^T$ .

TABLE X  
SRCC RESULTS ON TID2013 [53], SPAQ [54], AND AGIQA-3K [55] DATASETS ALONG WITH THE MEAN WEIGHTINGS FOR ALL PREDICTION HEADS. A VARIANT OF RESNET-18 IS USED AS THE BACKBONE NETWORK

Dataset	Mean Weightings							SRCC
	LIVE	CSIQ	BID	LIVE Challenge	KoniQ-10K	KADID-10K		
TID2013	0.241	0.138	0.042	0.147	0.114	0.318	0.700	
SPAQ	0.076	0.092	0.146	0.206	0.377	0.102	0.817	
AGIQA-3K	0.141	0.106	0.050	0.437	0.135	0.130	0.615	

TABLE XI  
SRCC RESULTS ON TID2013 [53], SPAQ [54], AND AGIQA-3K [55] DATASETS UNDER THE CROSS-DATASET SETUP. ALL METHODS USE A VARIANT OF RESNET-50 AS THE BACKBONE NETWORK

Method	TID2013	SPAQ	AGIQA-3K
PQR [20]	0.528	0.808	0.642
HyperIQA [28]	0.482	0.772	0.628
CONTRIQUE [60]	0.318	0.637	0.601
TSN-IQA (ResNet-50)	<b>0.734</b>	<b>0.821</b>	<b>0.648</b>

TABLE XII  
PERFORMANCE COMPARISON OF TSN-IQA WITH DIFFERENT KG MECHANISMS IN TERMS OF mSRCC, mPSI, AND THE COMPUTATIONAL COMPLEXITY (CC).  $T$  STANDS FOR THE NUMBER OF LEARNED TASKS

Configuration	mSRCC	mPSI	CC
LwF-KG (as baseline)	0.801	0.900	1.0
TSN-IQA (with soft assignment)	0.846	0.916	$T$
TSN-IQA (with hard assignment)	0.817	0.903	1.0

From Table VIII, we identify a clear trend that datasets with similar distortion scenarios have relatively smaller divergence values. We then load each group of task-specific BN parameters (together with the corresponding prediction head), and test it on all datasets, by which we obtain pairwise SRCC results among all datasets  $\{\text{SRCC}\}_{i,j=1}^T$  (see Table IX). Finally, we are able to measure the correlation between the learned BN parameters and the performance variations with an SRCC of  $-0.776$  between  $\{\text{SRCC}\}_{i,j=1}^T$  and  $\{\text{KL}\}_{i,j=1}^T$ . This provides empirical evidence that the more similar the datasets are in distortion scenarios, the better the inter-dataset prediction accuracy.

2) *Generalizability Analysis*: To empirically verify that TSN-IQA can be used to predict the perceptual quality of images beyond all seen datasets, we test the model learned in chronological order of the six tasks on three additional datasets, including TID2013 [53], SPAQ [54] and AGIQA-3K [55]. We report the SRCC results and the average weightings computed by the KG module over all images in Table X, from which we have two useful observations. First, the proposed TSN-IQA presents reasonable generalizability to the tasks it is not exposed to. Second, the KG module assigns perceptually meaningful weightings to the prediction heads. Specifically, the prediction heads learned on LIVE, CSIQ, and KADID-10K are assigned higher weightings when handling TID2013, containing multiple synthetic distortions. Similarly, the prediction heads for BID, LIVE Challenge, and KoniQ-10K are assigned higher weightings for SPAQ, which is dominated by realistic camera distortions. The situation becomes a little intricate on AGIQA-3K, a new dataset com-

prising artificially generated images. All prediction heads are assigned non-trivial weightings, exposing the uncertainty of TSN-IQA in handling this novel image type. We also compare TSN-IQA with three recent BIQA methods, *i.e.*, PQR [20], HyperIQA [28], and CONTRIQUE [60], following the same cross-dataset evaluation setup. As shown in Table XI, TSN-IQA outperforms other BIQA models on all three datasets, especially on TID2013 [53] that contains synthetic distortions. Nevertheless, there remains considerable room for improvement in quality prediction of artificially-generated images that exhibit substantial subpopulation shift.

3) *Computational Complexity Analysis*: We compare the computational complexity of TSN-IQA with LwF-KG [2]. The computation of a single forward pass for the two methods are identical. Specifically, given an image with a size of  $224 \times 224 \times 3$ , the number of multiply-accumulate operations (MACs) of TSN-IQA is about 18.2 G. After continually learned on  $T$  tasks, TSN-IQA computes  $T$  quality estimates with  $T$  groups of task-specific BN parameters during inference. As such, the computational complexity is linear with respect to the number of training tasks, which can be straightforwardly accelerated by parallel computing.

We have also tried a variant of the KG module that implements hard assignment by setting  $\tau = +\infty$ . With such a modification, only one forward pass is needed to compute the final quality score, which reduces the computational complexity by a factor of  $T$ . As shown in Table XII, although this computationally efficient variant delivers slightly inferior performance than the default TSN-IQA, it outperforms LwF-KG with the same computational complexity.

4) *Performance Stability*: We test the performance stability of TSN-IQA with respect to five different random initializations. As shown in Table XIII, TSN-IQA consistently demonstrates superior performance over other methods irrespective of the chosen backbone network.

## V. CONCLUSION AND DISCUSSION

We have introduced a simple yet effective method of continually learning BIQA models. The key to the success of the proposed TSN-IQA is to train task-specific BN parameters for each task while holding all pre-trained convolution filters fixed. On the one hand, TSN-IQA encourages more effective feature representation learning for different tasks. This is because BN participates all network stages of feature processing, which is better suited in the continual learning scenario for noticeably improved quality prediction accuracy, plasticity-stability trade-off, and task-length/order robustness. On the other hand, it permits a significant reduction in the number of parameters

TABLE XIII  
MEAN RESULTS (AND THE CORRESPONDING STANDARD DEVIATIONS) OF TSN-IQA AGAINST OTHER METHODS OVER FIVE RANDOM INITIALIZATIONS

Backbone	Method	mSRCC	mPI	mSI	mPSI
ResNet-18	SL	0.695 ( $\pm$ 0.018)	0.852 ( $\pm$ 0.005)	0.753 ( $\pm$ 0.004)	0.802 ( $\pm$ 0.003)
	SI	0.677 ( $\pm$ 0.116)	<b>0.856</b> ( $\pm$ 0.007)	0.868 ( $\pm$ 0.010)	0.862 ( $\pm$ 0.008)
	SI-KG	0.712 ( $\pm$ 0.086)	0.854 ( $\pm$ 0.008)	0.866 ( $\pm$ 0.019)	0.860 ( $\pm$ 0.013)
	MAS	0.717 ( $\pm$ 0.018)	0.854 ( $\pm$ 0.007)	0.865 ( $\pm$ 0.006)	0.859 ( $\pm$ 0.006)
	MAS-KG	0.747 ( $\pm$ 0.022)	0.853 ( $\pm$ 0.006)	0.871 ( $\pm$ 0.007)	0.862 ( $\pm$ 0.006)
	LwF	0.697 ( $\pm$ 0.026)	0.846 ( $\pm$ 0.004)	0.880 ( $\pm$ 0.011)	0.863 ( $\pm$ 0.007)
	LwF-KG	0.801 ( $\pm$ 0.003)	0.840 ( $\pm$ 0.003)	0.964 ( $\pm$ 0.003)	0.902 ( $\pm$ 0.002)
	TSN-IQA	<b>0.839</b> ( $\pm$ 0.004)	0.851 ( $\pm$ 0.003)	<b>0.983</b> ( $\pm$ 0.003)	<b>0.917</b> ( $\pm$ 0.001)
Backbone	Method	mSRCC	mPI	mSI	mPSI
Two-Stream DNN	SL	0.672 ( $\pm$ 0.016)	0.875 ( $\pm$ 0.005)	0.802 ( $\pm$ 0.008)	0.839 ( $\pm$ 0.004)
	SI	0.705 ( $\pm$ 0.021)	0.875 ( $\pm$ 0.005)	0.833 ( $\pm$ 0.008)	0.854 ( $\pm$ 0.005)
	SI-KG	0.799 ( $\pm$ 0.008)	0.862 ( $\pm$ 0.009)	0.948 ( $\pm$ 0.011)	0.905 ( $\pm$ 0.005)
	MAS	0.687 ( $\pm$ 0.043)	<b>0.877</b> ( $\pm$ 0.003)	0.826 ( $\pm$ 0.020)	0.851 ( $\pm$ 0.011)
	MAS-KG	0.806 ( $\pm$ 0.015)	0.865 ( $\pm$ 0.003)	0.950 ( $\pm$ 0.006)	0.908 ( $\pm$ 0.004)
	LwF	0.688 ( $\pm$ 0.019)	0.873 ( $\pm$ 0.011)	0.841 ( $\pm$ 0.008)	0.857 ( $\pm$ 0.009)
	LwF-KG	0.810 ( $\pm$ 0.009)	0.850 ( $\pm$ 0.008)	0.979 ( $\pm$ 0.001)	0.914 ( $\pm$ 0.004)
	TSN-IQA	<b>0.839</b> ( $\pm$ 0.009)	0.858 ( $\pm$ 0.005)	<b>0.981</b> ( $\pm$ 0.004)	<b>0.920</b> ( $\pm$ 0.004)

used for the KG mechanism, which only needs to replace a set of BN parameters.

TSN-IQA relies on five desiderata as specified in [2], among which the assumption of a common perceptual scale is foremost. It is well-known that the perceived quality of a visual image depends not only on the image content itself, but also on the subjective testing protocols as well as viewing conditions. For example, switching from single-stimulus methods to 2AFC approaches generally improves the accuracy of fine-grained quality annotations. We take this into consideration by pursuing binary labels as ground-truths. Moreover, the visibility of some distortions (e.g., JPEG compression) varies with the effective viewing distance. Although it would be ideal to give a complete treatment of viewing conditions (e.g., as part of the model input), our computational study shows the possibility to learn a common perceptual scale for different IQA datasets with MOSs collected under similar viewing conditions and having overlapping quality ranges. With the explosive growth of user-generated and computer-generated images, it is also desirable to perform online continual learning for BIQA, where there is no distinct boundaries between tasks (or datasets) during training.

#### ACKNOWLEDGMENT

This work was supported in part by Shanghai Municipal Science and Technology Major Project (2021SHZDZX0102), the Fundamental Research Funds for the Central Universities, the National Natural Science Foundation of China under Grants 61901262, 62371283, 62071407, and U19B2035, and the Hong Kong RGC Early Career Scheme (9048212).

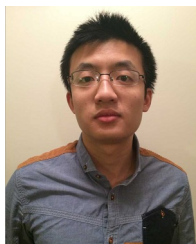
#### REFERENCES

- [1] Z. Wang and A. C. Bovik, *Modern Image Quality Assessment*. Morgan & Claypool, 2006.
- [2] W. Zhang, D. Li, C. Ma, G. Zhai, X. Yang, and K. Ma, "Continual learning for blind image quality assessment," *IEEE Transactions on Pattern Analysis and Machine Intelligence*, vol. 45, no. 3, pp. 2864–2878, Mar. 2023.
- [3] J. Liu, W. Zhou, X. Li, J. Xu, and Z. Chen, "LIQA: Lifelong blind image quality assessment," *IEEE Transactions on Multimedia*, vol. 25, pp. 5358–5373, Jul. 2022.
- [4] Z. Wang, H. R. Sheikh, and A. C. Bovik, "No-reference perceptual quality assessment of JPEG compressed images," in *IEEE International Conference on Image Processing*, vol. 1, 2002, pp. 477–480.
- [5] H. R. Sheikh, M. F. Sabir, and A. C. Bovik, "A statistical evaluation of recent full reference image quality assessment algorithms," *IEEE Transactions on Image Processing*, vol. 15, no. 11, pp. 3440–3451, Nov. 2006.
- [6] A. Mittal, A. K. Moorthy, and A. C. Bovik, "No-reference image quality assessment in the spatial domain," *IEEE Transactions on Image Processing*, vol. 21, no. 12, pp. 4695–4708, Dec. 2012.
- [7] D. Jayaraman, A. Mittal, A. K. Moorthy, and A. C. Bovik, "Objective quality assessment of multiply distorted images," in *Signals, Systems and Computers*, 2013, pp. 1693–1697.
- [8] L. Kang, P. Ye, Y. Li, and D. Doermann, "Convolutional neural networks for no-reference image quality assessment," in *IEEE Conference on Computer Vision and Pattern Recognition*, 2014, pp. 1733–1740.
- [9] J. L. McClelland, B. L. McNaughton, and R. C. O'Reilly, "Why there are complementary learning systems in the hippocampus and neocortex: Insights from the successes and failures of connectionist models of learning and memory," *Psychological Review*, vol. 102, no. 3, pp. 419–457, Jul. 1995.
- [10] M. McCloskey and N. J. Cohen, "Catastrophic interference in connectionist networks: The sequential learning problem," in *Psychology of Learning and Motivation*, 1989, pp. 109–165.
- [11] W. Zhang, K. Ma, G. Zhai, and X. Yang, "Uncertainty-aware blind image quality assessment in the laboratory and wild," *IEEE Transactions on Image Processing*, vol. 30, pp. 3474–3486, Mar. 2021.
- [12] Z. Li and D. Hoiem, "Learning without forgetting," *IEEE Transactions on Pattern Analysis and Machine Intelligence*, vol. 40, no. 12, pp. 2935–2947, Dec. 2018.
- [13] M. De Lange, R. Aljundi, M. Masana, S. Parisot, X. Jia, A. Leonardis, G. Slabaugh, and T. Tuytelaars, "A continual learning survey: Defying forgetting in classification tasks," *IEEE Transactions on Pattern Analysis and Machine Intelligence*, vol. 44, no. 7, pp. 3366–3385, Feb. 2021.
- [14] J. Yoon, S. Kim, E. Yang, and S. J. Hwang, "Scalable and order-robust continual learning with additive parameter decomposition," in *International Conference on Learning Representations*, 2020.
- [15] S. Ioffe and C. Szegedy, "Batch normalization: Accelerating deep network training by reducing internal covariate shift," in *International Conference on Machine Learning*, vol. 37, 2015, pp. 448–456.
- [16] A. Mittal, R. Soundararajan, and A. C. Bovik, "Making a 'completely blind' image quality analyzer," *IEEE Signal Processing Letters*, vol. 20, no. 3, pp. 209–212, Mar. 2013.
- [17] A. K. Moorthy and A. C. Bovik, "Blind image quality assessment: From natural scene statistics to perceptual quality," *IEEE Transactions on Image Processing*, vol. 20, no. 12, pp. 3350–3364, Dec. 2011.
- [18] D. Ghadiyaram and A. C. Bovik, "Perceptual quality prediction on authentically distorted images using a bag of features approach," *Journal of Vision*, vol. 17, no. 1, pp. 32–59, Jan. 2017.
- [19] S. Bosse, D. Maniry, K. R. Müller, T. Wiegand, and W. Samek, "Deep neural networks for no-reference and full-reference image quality

- assessment,” *IEEE Transactions on Image Processing*, vol. 27, no. 1, pp. 206–219, Jan. 2018.
- [20] H. Zeng, L. Zhang, and A. C. Bovik, “Blind image quality assessment with a probabilistic quality representation,” in *IEEE International Conference on Image Processing*, 2018, pp. 609–613.
- [21] X. Liu, J. v. d. Weijer, and A. D. Bagdanov, “RankQA: Learning from rankings for no-reference image quality assessment,” in *IEEE International Conference on Computer Vision*, 2017, pp. 1040–1049.
- [22] K. Ma, W. Liu, K. Zhang, Z. Duanmu, Z. Wang, and W. Zuo, “End-to-end blind image quality assessment using deep neural networks,” *IEEE Transactions on Image Processing*, vol. 27, no. 3, pp. 1202–1213, Mar. 2018.
- [23] K. Ma, X. Liu, Y. Fang, and E. P. Simoncelli, “Blind image quality assessment by learning from multiple annotators,” in *IEEE International Conference on Image Processing*, 2019, pp. 2344–2348.
- [24] A. Ciancio, E. A. B. da Silva, A. Said, R. Samadani, and P. Obrador, “No-reference blur assessment of digital pictures based on multifeature classifiers,” *IEEE Transactions on Image Processing*, vol. 20, no. 1, pp. 64–75, Jan. 2011.
- [25] D. Ghadiyaram and A. C. Bovik, “Massive online crowdsourced study of subjective and objective picture quality,” *IEEE Transactions on Image Processing*, vol. 25, no. 1, pp. 372–387, Jan. 2016.
- [26] V. Hosu, H. Lin, T. Sziranyi, and D. Saupe, “KonIQ-10k: An ecologically valid database for deep learning of blind image quality assessment,” *IEEE Transactions on Image Processing*, vol. 29, pp. 4041–4056, Jan. 2020.
- [27] W. Zhang, K. Ma, J. Yan, D. Deng, and Z. Wang, “Blind image quality assessment using a deep bilinear convolutional neural network,” *IEEE Transactions on Circuits and Systems for Video Technology*, vol. 30, no. 1, pp. 36–47, Jan. 2020.
- [28] S. Su, Q. Yan, Y. Zhu, C. Zhang, X. Ge, J. Sun, and Y. Zhang, “Blindly assess image quality in the wild guided by a self-adaptive hyper network,” in *IEEE Conference on Computer Vision and Pattern Recognition*, 2020, pp. 3664–3673.
- [29] H. Zhu, L. Li, J. Wu, W. Dong, and G. Shi, “MetaQA: Deep meta-learning for no-reference image quality assessment,” in *IEEE Conference on Computer Vision and Pattern Recognition*, 2020, pp. 14 131–14 140.
- [30] R. Ma, H. Luo, Q. Wu, K. N. Ngan, H. Li, F. Meng, and L. Xu, “Remember and reuse: Cross-task blind image quality assessment via relevance-aware incremental learning,” in *ACM International Conference on Multimedia*, 2021, pp. 5248–5256.
- [31] R. M. French, “Catastrophic forgetting in connectionist networks,” *Trends in Cognitive Sciences*, vol. 3, no. 4, pp. 128–135, Apr. 1999.
- [32] J. Kirkpatrick, R. Pascanu, N. Rabinowitz, J. Veness, G. Desjardins, A. A. Rusu, K. Milan, J. Quan, T. Ramalho, A. Grabska-Barwinska, C. Clopath, D. Kumaran, and R. Hadsell, “Overcoming catastrophic forgetting in neural networks,” *National Academy of Sciences*, vol. 114, no. 13, pp. 3521–3526, Mar. 2017.
- [33] C. V. Nguyen, Y. Li, T. D. Bui, and R. E. Turner, “Variational continual learning,” in *International Conference on Learning Representations*, 2018.
- [34] F. Zenke, B. Poole, and S. Ganguli, “Continual learning through synaptic intelligence,” in *International Conference on Machine Learning*, vol. 70, 2017, pp. 3987–3995.
- [35] R. Aljundi, F. Babiloni, M. Elhoseiny, M. Rohrbach, and T. Tuytelaars, “Memory aware synapses: Learning what (not) to forget,” in *European Conference on Computer Vision*, 2018, pp. 139–154.
- [36] C. Fernando, D. Banarse, C. Blundell, Y. Zwols, D. Ha, A. A. Rusu, A. Pritzel, and D. Wierstra, “PathNet: Evolution channels gradient descent in super neural networks,” *CoRR*, vol. abs/1701.08734, 2017.
- [37] A. Mallya, D. Davis, and S. Lazebnik, “Piggyback: Adapting a single network to multiple tasks by learning to mask weights,” in *European Conference on Computer Vision*, 2018, pp. 67–82.
- [38] A. Mallya and S. Lazebnik, “PackNet: Adding multiple tasks to a single network by iterative pruning,” in *IEEE Conference on Computer Vision and Pattern Recognition*, 2018, pp. 7765–7773.
- [39] A. A. Rusu, N. C. Rabinowitz, G. Desjardins, H. Soyer, J. Kirkpatrick, K. Kavukcuoglu, R. Pascanu, and R. Hadsell, “Progressive neural networks,” *CoRR*, vol. abs/1606.04671, 2016.
- [40] P. Singh, V. K. Verma, P. Mazumder, L. Carin, and P. Rai, “Calibrating CNNs for lifelong learning,” in *Advances in Neural Information Processing Systems*, 2020, pp. 15 579–15 590.
- [41] M. Carandini and D. J. Heeger, “Normalization as a canonical neural computation,” *Nature Reviews Neuroscience*, vol. 13, no. 1, pp. 51–62, Nov. 2012.
- [42] L. Huang, J. Qin, Y. Zhou, F. Zhu, L. Liu, and L. Shao, “Normalization techniques in training DNNs: Methodology, analysis and application,” *CoRR*, vol. abs/2009.12836, 2020.
- [43] C. Xie, M. Tan, B. Gong, J. Wang, A. L. Yuille, and Q. V. Le, “Adversarial examples improve image recognition,” in *IEEE Conference on Computer Vision and Pattern Recognition*, 2020, pp. 819–828.
- [44] Y. Li, N. Wang, J. Shi, J. Liu, and X. Hou, “Revisiting batch normalization for practical domain adaptation,” in *IEEE International Conference on Learning Representations*, 2017.
- [45] W.-G. Chang, T. You, S. Seo, S. Kwak, and B. Han, “Domain-specific batch normalization for unsupervised domain adaptation,” in *IEEE Conference on Computer Vision and Pattern Recognition*, 2019, pp. 7354–7362.
- [46] V. Dumoulin, J. Shlens, and M. Kudlur, “A learned representation for artistic style,” in *International Conference on Learning Representations*, 2017.
- [47] D. Ulyanov, A. Vedaldi, and V. Lempitsky, “Instance normalization: The missing ingredient for fast stylization,” *CoRR*, vol. abs/1607.08022, 2016.
- [48] J. Zhang, D. Chen, J. Liao, W. Zhang, G. Hua, and N. Yu, “Passport-aware normalization for deep model protection,” in *Advances in Neural Information Processing Systems*, vol. 33, 2020, pp. 22 619–22 628.
- [49] L. L. Thurstone, “A law of comparative judgment,” *Psychological Review*, vol. 34, pp. 273–286, Jul. 1927.
- [50] R. A. Bradley and M. E. Terry, “Rank analysis of incomplete block designs: I. The method of paired comparisons,” *Biometrika*, vol. 39, pp. 324–345, Dec. 1952.
- [51] M.-F. Tsai, T.-Y. Liu, T. Qin, H.-H. Chen, and W.-Y. Ma, “FRank: A ranking method with fidelity loss,” in *International ACM SIGIR Conference on Research and Development in Information Retrieval*, 2007, pp. 383–390.
- [52] S. P. Lloyd, “Least squares quantization in PCM,” *IEEE Transactions on Information Theory*, vol. 28, no. 2, pp. 129–137, Mar. 1982.
- [53] P. Nikolay, J. Lina, I. Oleg, L. Vladimir, E. Karen, A. Jaakko, V. Benoit, C. Kacem, C. Marco, B. Federica, and C.-C. J. Kuo, “Image database TID2013: Peculiarities, results and perspectives,” *Signal Processing: Image Communication*, vol. 30, pp. 57–77, Jan. 2015.
- [54] Y. Fang, H. Zhu, Y. Zeng, K. Ma, and Z. Wang, “Perceptual quality assessment of smartphone photography,” in *IEEE Conference on Computer Vision and Pattern Recognition*, 2020, pp. 3677–3686.
- [55] C. Li, Z. Zhang, H. Wu, W. Sun, X. Min, X. Liu, G. Zhai, and W. Lin, “AGIQA-3K: An open database for AI-generated image quality assessment,” *IEEE Transactions on Circuits and Systems for Video Technology*, to appear, 2023.
- [56] E. C. Larson and D. M. Chandler, “Most apparent distortion: Full-reference image quality assessment and the role of strategy,” *Journal of Electronic Imaging*, vol. 19, no. 1, pp. 1–21, Jan. 2010.
- [57] H. Lin, V. Hosu, and D. Saupe, “KADID-10k: A large-scale artificially distorted IQA database,” in *International Conference on Quality of Multimedia Experience*, 2019, pp. 1–3.
- [58] K. He, X. Zhang, S. Ren, and J. Sun, “Deep residual learning for image recognition,” in *IEEE Conference on Computer Vision and Pattern Recognition*, 2016, pp. 770–778.
- [59] D. Kingma and J. Ba, “Adam: A method for stochastic optimization,” in *International Conference on Learning Representations*, 2015.
- [60] P. C. Madhusudana, N. Birkbeck, Y. Wang, B. Adsumilli, and A. C. Bovik, “Image quality assessment using contrastive learning,” *IEEE Transactions on Image Processing*, vol. 31, pp. 4149–4161, Jun. 2022.
- [61] K. Simonyan and A. Zisserman, “Very deep convolutional networks for large-scale image recognition,” in *International Conference on Learning Representations*, 2015.



**Weixia Zhang** (Member, IEEE) received the B.E. degree from the Wuhan University, Wuhan, China, in 2011 and the M.S. degree in electrical and computer engineering from the University of Rochester, NY, USA, in 2013. He then received the Ph.D. degree from the Wuhan University, Wuhan, China, in 2018. He is currently an Associate Research Scientist with the MoE Key Lab of Artificial Intelligence, AI Institute, Shanghai Jiao Tong University. His research interests include perceptual quality evaluation and enhancement.



**Kede Ma** (Senior Member, IEEE) received the B.E. degree from the University of Science and Technology of China, Hefei, China, in 2012, and the M.S. and Ph.D. degrees in electrical and computer engineering from the University of Waterloo, Waterloo, ON, Canada, in 2014 and 2017, respectively. He was a Research Associate with the Howard Hughes Medical Institute and New York University, New York, NY, USA, in 2018. He is currently an Assistant Professor with the Department of Computer Science, City University of Hong Kong. His research interests

include perceptual image processing, computational vision, and computational photography.



**Guangtao Zhai** (Senior Member, IEEE) received the B.E. and M.E. degrees from Shandong University, Shandong, China, in 2001 and 2004, respectively, and the Ph.D. degree from Shanghai Jiao Tong University, Shanghai, China, in 2009, where he is currently a Research Professor with the Institute of Image Communication and Information Processing. From 2008 to 2009, he was a Visiting Student with the Department of Electrical and Computer Engineering, McMaster University, Hamilton, ON, Canada, where he was a Post-Doctoral Fellow from

2010 to 2012. From 2012 to 2013, he was a Humboldt Research Fellow with the Institute of Multimedia Communication and Signal Processing, Friedrich Alexander University of Erlangen-Nuremberg, Germany. He received the Award of National Excellent Ph.D. Thesis from the Ministry of Education of China in 2012. His research interests include multimedia signal processing and perceptual signal processing.



**Xiaokang Yang** (Fellow, IEEE) received the B.S. degree from Xiamen University, Xiamen, China, in 1994, the M.S. degree from the Chinese Academy of Sciences, Shanghai, China, in 1997, and the Ph.D. degree from Shanghai Jiao Tong University, Shanghai, in 2000. From September 2000 to March 2002, he worked as a Research Fellow with the Centre for Signal Processing, Nanyang Technological University, Singapore. From April 2002 to October 2004, he was a Research Scientist with the Institute for Infocomm Research (I2R), Singapore. From August

2007 to July 2008, he visited the Institute for Computer Science, University of Freiburg, Germany, as an Alexander von Humboldt Research Fellow. He is currently a Distinguished Professor with the School of Electronic Information and Electrical Engineering, Shanghai Jiao Tong University. He has published over 200 refereed articles and has filed 60 patents. His current research interests include image processing and communication, computer vision, and machine learning. He is an Associate Editor of the IEEE TRANSACTIONS ON MULTIMEDIA.